Marine Research
of the National Academy of Marine Research
ISSN: 2709-6629 (Vol.3 Iss.1)
GPN: 2011200033

DOI: http://dx.doi.org/10.29677/MR.202306_3(1).0002
2023, 3(1), 21-42

Establishment and Application of Taiwan's First Marine Data Buoy for In Situ Automated Gamma Radioactivity Monitoring: A Case Study of Cesium-137 and Bismuth-214

Bo-Shian Wang [1*] Christos Tsabaris [2] Ke-Hsien Fu [1] Wen-Chang Yang [1]
Sheng-Hsueh Chen [3] Mong-Hsien Shih [3] Chien-Ming Lee [3] Yi-Fang Lee [1]
Kun-I Lin [1] Kuo-Ching Jao [3]

[1] National Academy of Marine Research (NAMR), Ocean Affairs Council, Taiwan
[2] Hellenic Centre for Marine Research (HCMR), Institute of Oceanography, Greece
[3] Coastal Ocean Monitoring Center (COMC), National Cheng Kung University, Taiwan

ABSTRACT

To establish a technology for near-continuous and near-real-time monitoring of marine radioactivity and to enhance early warning of abnormal radioactivity in the ocean, we constructed a marine in situ automated gamma radioactivity monitoring buoy station off the northeastern coast of Yilan, Taiwan, in 2022. The data is transmitted via 4G and automatically converted into activity concentrations using an automatic alarm module that determines and issues threshold concentration alerts, thus establishing a comprehensive procedure for marine radioactivity alarms. Data reliability was ensured through the use of the naturally occurring nuclide ^{40}K. During the monitoring period, from August to December 2021, activity concentrations of the anthropogenic nuclide ^{137}Cs remained consistently below the instrumental detection limit. This observation provides conclusive evidence of the absence of safety concerns related to ^{137}Cs contamination in the seawater off the coast of Yilan. Furthermore, the dose rates of naturally occurring nuclide ^{214}Bi exhibited a correlation with precipitation, especially during rainfalls caused by typhoons passing through the buoy deployment area and the East Asian Monsoon in winter. However, for typhoon-induced precipitation events that did not traverse the study area, substantial amounts of ^{214}Bi were generated, yet no significant relationship was observed between the rainfall amount and the corresponding ^{214}Bi activity concentration. The underlying mechanism behind this preliminary observation requires further investigation.

Keywords: Marine gamma radioactivity, cesium-137, bismuth-214, data buoy, automated monitoring.

* Corresponding author, e-mail: bswang@namr.gov.tw

Received 19 July 2023, Accepted 26 September 2023.

1 INTRODUCTION

The ocean encompasses three-quarters of the Earth's surface and serves as the ultimate repository for various substances, including anthropogenic radioactive materials. These materials exist in solid, liquid, and gaseous forms and enter the ocean through processes such as atmospheric deposition, rainfall or snowfall, rivers or glaciers, and submarine groundwater (Buesseler et al., 2016; Povinec & Hirose, 2012). Anthropogenic radioactive substances released into the ocean, whether actively (e.g., nuclear testing, emissions from nuclear power plants) or passively (e.g., nuclear power plant accidents, leakage, or disposal of radioactive waste), disperse, suspend, settle, or associate with particles in the ocean, manifesting as ions and colloids, encountering particle adsorption and biological uptake processes (Santschi, 2018).

The radioactive isotopes present in the ocean are primarily of natural origin. The most abundant isotope is potassium-40 (^{40}K, with a half-life of 1.25×10^9 years and an activity concentration of approximately 11,000 to 14,000 Bq m^{-3}), followed by uranium-238 (^{238}U, with a half-life of 4.67×10^9 years and an activity concentration of approximately 40 Bq m^{-3}). The total activities of these two isotopes in seawater, calculated based on the total volume, are approximately 1.5×10^7 PBq and 3.7×10^4 PBq, respectively (Buesseler, 2014). In comparison, the total quantity of anthropogenically produced radioactive isotopes is considerably smaller. These isotopes are primarily the result of nuclear testing since the 1950s, the Three Mile Island nuclear power plant accident in 1979, the Chernobyl nuclear power plant accident in 1986, and the Fukushima Daiichi nuclear power plant accident in 2011. For instance, the total activity of cesium-137 (^{137}Cs, with a half-life of 30.2 years) is approximately 1.1×10^3 PBq (Buesseler, 2014). However, certain anthropogenic radionuclides tend to be readily absorbed and accumulated by organisms (Topcuoğlu, 2001; Tracy et al., 2013). Through the growth of organisms and transfers within the food chain, they continue to accumulate, posing adverse implications for food safety in fisheries and the health and safety of recreational activities in marine areas. Therefore, regular monitoring of anthropogenic radiation background in the ocean is essential.

To enable real-time monitoring of marine radioactivity pollution and prompt responses, the development of in situ automated detection instruments for ocean radioactivity has advanced since the 1990s. Radioactive isotopes emit three types of radiation: alpha (α), beta (β), and gamma (γ) radiation. Alpha and beta radiation have limited ranges in water due to ionization and elastic scattering and are undetectable in situ. In contrast, gamma radiation possesses substantial penetration power and can be used to identify the activity concentration of specific nuclides by detecting characteristic gamma energy spectra. Based on their mechanism, radiation detectors can be categorized into scintillation detectors, ionization detectors, and semiconductor detectors. Currently, the most widely used detectors for gamma spectrum detection are high purity germanium semiconductor (HPGe) detectors and scintillation detectors such as sodium iodide (NaI(Tl)) or lanthanum bromide ($LaBr_3$) detectors (Dou et al., 2021; Kwak et al., 2017). HPGe detectors provide exceptional energy resolution; however, they require controlled working environments and are characterized by large equipment sizes. As a result, they are more aptly utilized for high-precision laboratory analysis, rather than for continuous and extended in situ monitoring. $LaBr_3$ detectors possess higher energy resolution (approximately 3%) compared to NaI(Tl) detectors (approximately 7%), but exhibit lower detection efficiency and more stringent working environment requirements, including inherent spectral interference from $LaBr_3$. Consequently, NaI(Tl) detectors remain the mainstream choice for environmental field applications and commercially available instrument products (Povinec & Hirose, 2012). Gamma radiation detectors using NaI(Tl) crystals as probes currently dominate international marine gamma radiation monitoring due to their relatively high detection efficiency, lower working environment thresholds, cost-effectiveness, and compact size advantages (Kumagai et al., 2012; Pensieri et al., 2018; Ren et al., 2017).

Marine Research of the National Academy of Marine Research
DOI: 10.29677/MR.202306_3(1).0002

Considering the absence of automated real-time radiation monitoring technology in Taiwan's oceanic areas, the National Academy of Marine Research has introduced marine gamma spectrometers and related technology through international collaboration. By integrating this technology with established buoy technology, a preliminary gamma radioactivity mooring buoy station has been established off the northeastern coast of Yilan (121°55' 33"E, 24°57'3"N), Taiwan (Figure 1). This station serves two purposes: conducting preliminary experiments for automated gamma radioactivity monitoring and enhancing the Taiwanese government's capabilities in ocean radioactivity monitoring and early pollution warning.

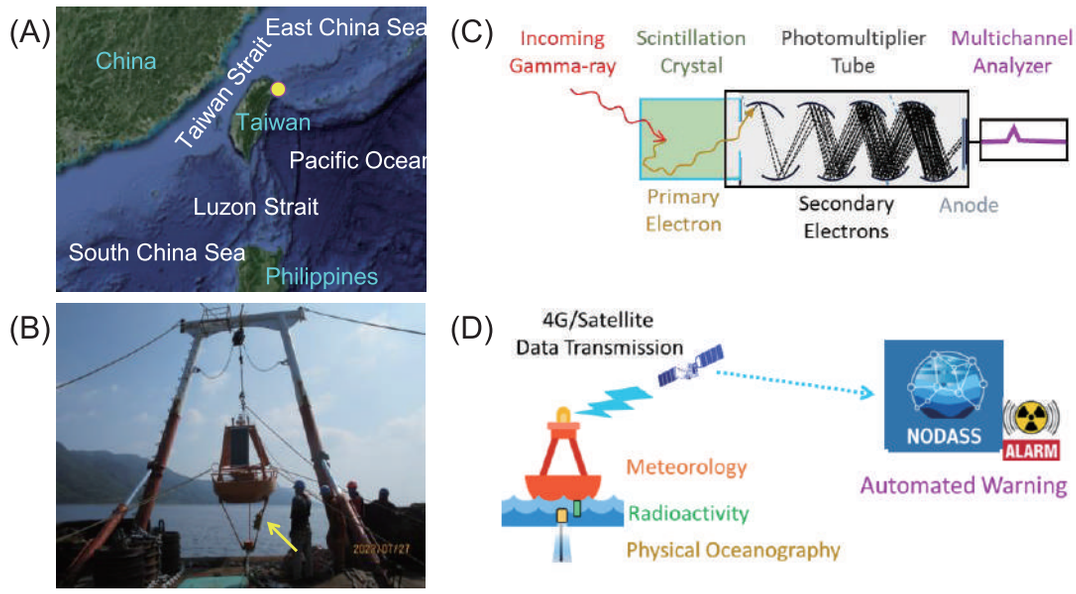

Figure 1. (A) Location of the gamma radioactivity monitoring buoy (marked with a yellow dot) off the northeastern coast of Yilan, Taiwan; (B) Deployment of the in situ automated gamma radioactivity monitoring buoy (the arrow indicates the position of the gamma spectrometer); (C) Fundamental working principle of gamma spectrometry; (D) Data transfer process in our system. The NODASS platform is responsible for data storage and automatic radiation exceeding standard warnings.

2 MATERIALS AND METHODS

2.1 Overview of marine radioactivity monitoring in Taiwan

The anthropogenic radioactive substances present in the waters surrounding Taiwan primarily originate from nuclear testing and are transported by ocean currents (Aoyama et al., 2008; Huang et al., 2021; Wu, 2018). They are less directly affected by the three major international nuclear accidents mentioned earlier. As time progresses, radioactive isotopes generated during the nuclear testing era naturally decay, allowing the ocean to gradually return to its normal state (Inomata et al., 2008).

Furthermore, Taiwan operated three nuclear power plants between the 1970s and 1980s. However, the Taiwanese government has been actively promoting energy transition and electricity industry reform policies since 2016, with the goal of achieving a "nuclear-free homeland" by 2025. Two nuclear power plants have already been shut down and are in the process of decommissioning. Nevertheless, Taiwan is not entirely within a nuclear-free safety environment. The rapid economic development of China in the 21st century has led to a significant increase in electricity demand, resulting in the construction of numerous power plants, including nuclear power facilities. Currently, there are more than twenty nuclear power plants situated along the coastal regions of China, with particularly high concentration in the southeastern coastal cities (Yu et al., 2020).

Marine Research of the National Academy of Marine Research
DOI: 10.29677/MR.202306_3(1).0002

The presence of numerous nuclear power plants along the Chinese coast heightens the potential for anthropogenic radioactive pollution in the Taiwan Strait, posing potential risks to the Taiwanese population in terms of marine recreational activities, fisheries, and seafood consumption. Of particular concern is China's lack of transparency regarding its nuclear safety incidents. For instance, (1) the Fuqing Nuclear Power Plant in Fujian Province experienced abnormalities in June and October 2020, leading to the shutdown of its generating units. The occurrence of radiation leakage remains uncertain, even though the plant is located only 162 kilometers away from Miaoli in Central Taiwan. (2) The Taishan Nuclear Power Plant in Guangdong Province was reported to have experienced fuel rod damage resulting in radiation leakage in June 2021. Given the quantity of nuclear power plants along the Chinese coast and the lack of transparency, it is imperative for Taiwan to develop a real-time monitoring and early warning system for radiation in its marine areas to enable prompt responses in the event of a nuclear safety incident.

2.2 Gamma spectrometer used in this study

The operational principle of gamma spectrometry relies on the phenomenon of photon generation when gamma particles within seawater interact with a scintillation crystal, producing photons in direct proportion to the energy of the gamma particles (Figure 1C). These photons subsequently impinge upon a photomultiplier tube, where they undergo conversion into electronic signals and amplification. These electronic signals are further processed into voltage pulse signals, directly proportional to the energy of the gamma particles. Ultimately, the integral of the characteristic energy peaks, acquired through multi-channel energy spectrum analysis, furnishes the energy intensity of specific nuclides. Furthermore, the instrument's sensing area requires sealing within a watertight metallic structure for protection, and it is coated with anti-biofouling plastic material. The framework is constructed from anti-corrosion stainless steel SUS316, with joints designed for underwater plugging and unplugging, permitting replacement of the radiation detection instrument underwater when necessary.

In this study, we opted for a NaI(Tl) crystal, characterized by its relatively high luminous efficiency, low detection technology threshold, and cost-effectiveness (KATERINA II, standard model, manufactured by HORST) (Pensieri et al., 2018). This underwater gamma-ray spectrometer can detect both natural and anthropogenic radioactive nuclides. The NaI(Tl) scintillation crystal, in its standard configuration, measures 7.62×7.62 cm and encompasses 1,024 spectral channels for analyzing the energy spectrum range of gamma radioactivity, spanning from 50 to 2,800 KeV. For ^{137}Cs (with a peak energy of approximately 661 KeV), the instrument exhibits a detection resolution of approximately 6.5% and a lower detection limit of approximately 30 Bq m^{-3}. It remains operational at a maximum underwater depth of 400 meters. While the detection limit for ^{137}Cs of the KATERINA II exceeds that of the surrounding seawaters in Taiwan and the Western Pacific (approximately 1.0±0.5 Bq m^{-3}) (Huang et al., 2021), the instrument is highly sensitive and can monitor radioactivity levels that breach the criteria specified by both the Atomic Energy Council's Environmental Radiation Monitoring Regulations (<2,000 Bq m^{-3}) and the World Health Organization (WHO) drinking water standard (<10,000 Bq m^{-3}).

To facilitate system calibration and maintenance during the trial operation phase, the gamma radiation detection instrument in this project will be positioned on the lower bracket of the buoy, located 1.5 meters below the sea surface. Natural radioactive nuclide ^{40}K (with a primary peak at 1,460 KeV) and the gross count of gamma radioactivity will serve as references for assessing the gamma spectrometer's performance, considering the experimental field conditions. For this study, the gamma spectrometer on the buoy will be configured to continuously transmit integrated gamma spectrum data at one-hour intervals. The integrated counting values for a day (24 hours) will then be converted into activity concentrations, based on the integrated values of the characteristic peaks of each nuclide in the spectrum.

Marine Research of the National Academy of Marine Research
DOI: 10.29677/MR.202306_3(1).0002

2.3 Features of the in situ automated gamma radioactivity monitoring buoy

The real-time gamma radioactivity monitoring buoy system, to be established for this study, comprises three essential components: a radioactivity detection instrument, a data buoy, and a data processing backend (Figure 2). The buoy is constructed from aluminum alloy, with a diameter of 1.8 meters. Positioned atop the base of the buoy are three 90-watt solar panels, serving to provide the required long-term operational power for observations. Additionally, the buoy system incorporates warning lights and radar reflectors to notify nearby vessels and prevent potential collisions. The gamma radiation detector is affixed to the lower bracket of the buoy, positioned approximately two meters below the water's surface. The detected gamma radiation values of seawater are retrieved by the data acquisition system aboard the buoy, configured to record data at hourly intervals by default. The gamma spectrum data, in conjunction with latitude and longitude coordinates and system voltage, are transmitted in near real time to the onshore data monitoring station through the data transmission equipment of the buoy, utilizing 4G as the primary communication method, with Iridium satellite transmission as a secondary option (Figure 1D).

This buoy-based observation technology has been operational in Taiwan for decades, undergoing significant technical development, and has been primarily employed for marine meteorological observations (Kao et al., 2003). The key advantage of utilizing this buoy lies in its substantial size, affording increased buoyancy and ample space for the necessary solar panels and battery systems for power supply, as well as facilitating the installation of surface and underwater scientific instruments. The buoy system itself possesses real-time transmission capabilities, enabling the regular transmission of instrument detection values to onshore receiving stations through 4G or satellite communication. To ensure data integrity, the buoy is equipped with a data logger, serving as a backup mechanism to safeguard data in the event of communication disruptions.

Within this system configuration, an additional gamma spectrometer is installed to monitor anthropogenic radioactive nuclides, such as ^{137}Cs, along with natural radionuclides including ^{40}K, bismuth-214 (^{214}Bi), and lead-214 (^{214}Pb), spanning the entire gamma energy spectrum. The anchoring of the buoy system relies on robust iron chains characterized by a higher working load capacity. To reduce the weight of these iron chains underwater, the system employs a taut mooring design, ensuring that the communication and charging devices positioned atop the buoy remain at the sea surface, thereby maintaining efficient communication transmission and solar panel charging. Two sizes of iron chains, measuring 19 cm and 26 cm, are employed, boasting a maximum tensile strength capable of withstanding extreme conditions, such as waves and currents, providing a safety factor of more than two. These iron chains undergo hot-dip galvanization to ensure corrosion resistance in seawater for up to 1.5 years. The anchoring system comprises three sets of 1.2-ton train wheels, boasting a total weight exceeding 3.6 tons, equipped to withstand typhoons and the formidable waves commonly encountered in the Western Pacific Ocean.

DOI: 10.29677/MR.202306_3(1).0002

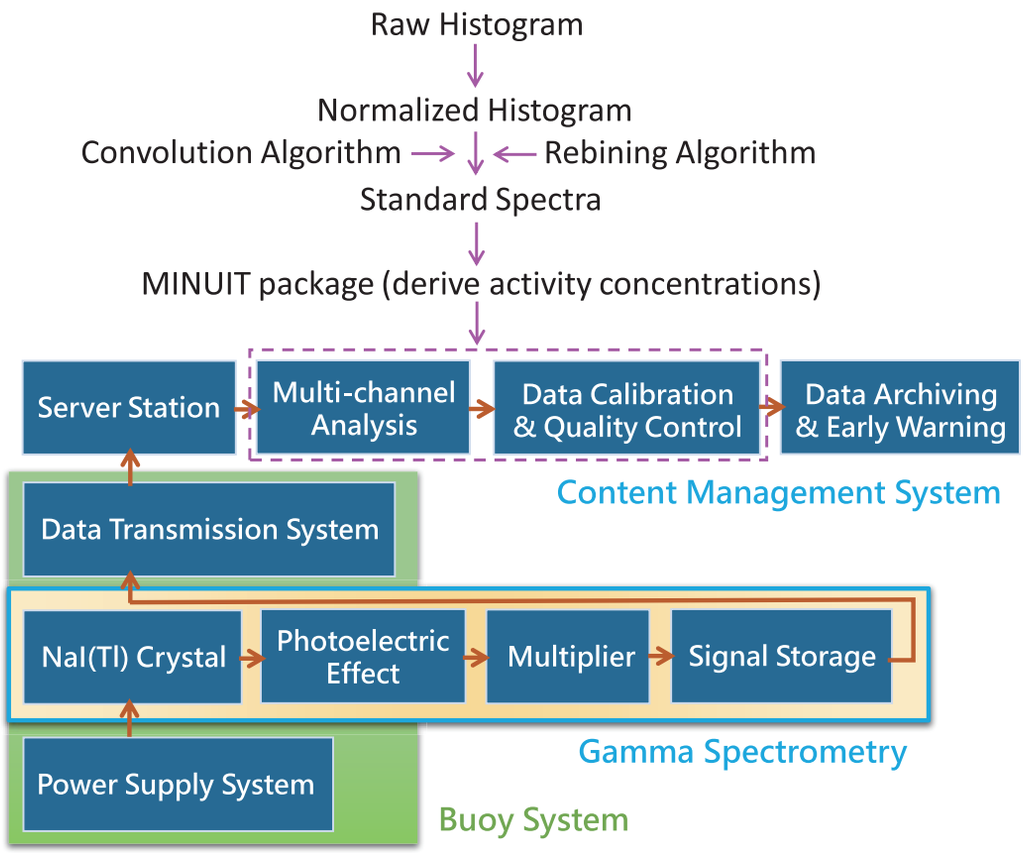

Figure 2. Schematic representation of the main components of the marine in situ automated gamma radioactivity monitoring buoy and the associated algorithms applied for data reduction.

2.4 Testing area, buoy deployment, and quality control

The selection of the site for setting up the near-real-time gamma radioactivity monitoring buoy in this study was informed by numerical simulations of the rate and extent of oceanic transport and dispersion of anthropogenic radionuclides during the 2011 Fukushima Daiichi nuclear disaster, in conjunction with in situ seawater radioactivity sampling data (Behrens et al., 2012; Buesseler et al., 2016; Burr et al., 2020; Kumamoto et al., 2017), as well as the three-dimensional spatial distribution of anthropogenic radionuclide activity concentrations in the Western Pacific (Aoyama et al., 2008; Men et al., 2015). Despite the reduction in activity due to dilution, particle removal, or radioactive decay during the dispersion of radioactive nuclides, materials released from the Fukushima coastal area in 2011 generally followed the surface circulation patterns of the North Pacific. If water carrying radioactive substances is transported by the Kuroshio Current to the eastern waters of Taiwan or even enters the southwestern waters of Taiwan via the Luzon Strait during winter, the journey would span approximately one to five years (Behrens et al., 2012). In the event that water carrying radioactive substances diffuses within mesoscale eddies during the initial phase of source dispersion, radioactive materials could reach the eastern waters of Taiwan and the entire Western Pacific within several months. Consequently, we have chosen Honeymoon Bay at the northeastern coast of Yilan, Taiwan, as the initial monitoring area for nuclear pollution, functioning as a "sentinel" (Figure 1A). This selection serves as a benchmark for assessing the potential presence of gamma-emitting radionuclides in wastewater released from the Fukushima Daiichi nuclear power plant in Japan. Furthermore, the site selection avoids the influence of gamma radiation releases from coastal nuclear power plants in China (Burr et al., 2020) and serves as a reference point for low gamma radiation background levels, relevant to future automatic radiation monitoring stations in the Taiwan Strait.

DOI: 10.29677/MR.202306_3(1).0002

The buoy deployment process involved using a maritime working vessel equipped with a rear A-frame capable of safely hoisting a minimum load of five tons, thus facilitating the lifting of the approximately 4-ton anchor (Figure 1B). Buoy deployment operations were conducted under sea state conditions of level 3 or below. The deployment sequence included the buoy, followed by the iron chain, with the anchor being released last. The quality control and operation of the buoy system and data adhered to the practices outlined by the National Data Buoy Center (NDBC) in the United States and the Quality Control and Operation Specifications for Data Buoys provided by the Central Weather Administration in Taiwan (Doong et al., 2007). In this study, the natural radionuclide ^{40}K served as the basis for evaluating the spectrum validation and data quality control of the gamma radiation detector. Upon confirming that both the gross count and radiation count of the ^{40}K peak in the gamma spectrum fell within normal ranges, the activity concentration (A) of each radionuclide could be calculated from the spectrum using Equation (1) presented below:

$$A\ (Bq/m^3)=\frac{CPS}{I_\gamma \times \varepsilon_m} \quad (1)$$

In Equation (1), CPS represents the integrated signal strength in the characteristic peak of a specific radionuclide per unit time, I_γ signifies the emission probability of gamma radiation, and ε_m denotes the detector efficiency in the marine environment (per cubic meter).

The determination of the minimum detectable amount (MDA) for each radionuclide in the gamma spectrometer relies on a 24-hour measurement conducted during rainy periods and a background spectrum recorded during non-rainy periods (absent precipitation events). This determination is accomplished through Equation (2):

$$MDA\ (Bq/m^3)=\frac{L_D}{\varepsilon_m \times I_\gamma \times T} \quad (2)$$

In this equation, L_D signifies the detection limit, T represents the detection time, I_γ denotes the emission probability of gamma radiation, and ε_m stands for the detector's efficiency in the marine environment (in cubic meters). The data reading and processing adhere to the procedures outlined for KATERINA II (Kalfas et al., 2016; Pensieri et al., 2018). This includes the utilization of SPECTRW software and its algorithms for the correction of background interference, Compton photons, and the overlapping energy peaks (Kalfas et al., 2016) (Figure 2).

DOI: 10.29677/MR.202306_3(1).0002

3 RESULTS AND DISCUSSION

3.1 Stability of in situ gamma radioactivity observation

The marine in situ automated gamma radioactivity monitoring buoy station, deployed off the northeastern coast of Yilan, has undergone a smooth 4-month trial operation, characterized by uninterrupted data transmission (as shown in Table 1). Given the exceedingly low activity concentration of anthropogenic radionuclides in the marine environment during typical periods, we have employed natural radionuclide ^{40}K as a reference for assessing the stability and data quality of the instrument's detection results (Figure 3A). This approach relies on the understanding that potassium constitutes one of the primary elements in seawater, with a concentration of 390±10 mg L^{-1}. It is considered a conservative element with generally stable concentration in seawater, except for the influence of rainfall or river inflow. In accordance with this premise, we have calculated the daily radioactivity concentration of ^{40}K, excluding data from rainy periods for comparison with existing literature, yielding a value of 12,212±195 Bq m^{-3} (mean±SD, SD denotes 1 standard deviation). This value aligns with the range of literature values, falling between 12,000 to 14,000 Bq m^{-3} (Bailly du Bois et al., 2020; Choi et al., 2023; Tsabaris et al., 2021); the observed 1.6% variation (1SD) in the non-rainfall ^{40}K data implies the stability of the detection capabilities of the instrument during non-rainfall periods, under the assumption that seawater salinity remains constant throughout this interval. Conversely, during rainfall periods, rainwater dilutes seawater salinity, resulting in a decrease in the ^{40}K activity concentration (Figure 3A). In the absence of rainfall, the gross gamma radiation count in surface seawater in the study area measured 33,608±620 Bq m^{-3} (mean±SD). This outcome not only affirms the proper functioning of the NaI(Tl) scintillation detector and photomultiplier tube, but underscores the instrument's stability by exhibiting only minimal variation of approximately 1.8% (1SD). This indicates that gamma radiation values in surface seawater in the study area during non-rainfall periods exhibit limited short-term variability, which closely approximates the systematic detection error of the instrument. The results, derived using ^{40}K and the total gamma radiation count, demonstrate that our instrument setup and spectral calculations can precisely and accurately determine the activity concentration of individual radionuclide energy peaks. Regrettably, this study lacks records of seawater salinity. Our future plans include the addition of a conductivity sensor to the data buoy, which will allow us to elucidate the relationship between ^{40}K and rainfall during precipitation events.

Like previous studies (Pensieri et al., 2018; Tsabaris et al., 2021), we have also observed that rainfall and seasonal variations in water temperature can impact gamma radiation counting and spectral energy. For instance, rainfall affects the ^{40}K signal primarily due to seawater potassium dilution by rainwater, leading to a reduction in the ^{40}K activity concentration. Furthermore, some atmospheric gamma radiation enters the surface seawater, partially overlapping with the ^{40}K peak in the spectrum (Patiris et al., 2021). Temperature variations induce spectral drift, an inherent challenge in scintillation gamma spectrum techniques, as temperature fluctuations can result in voltage variations within the instrument, thereby influencing energy distribution in the spectrum (Pensieri et al., 2018). The KATERINA II gamma spectrometer employed in this study featured digital electronics within its electronic module, allowing the compensation of spectrum variations caused by voltage drift. This mechanism adjusted the voltage output for strong peaks, effectively mitigating significant effects over short periods of time (e.g., a few hours). However, seasonal surface water temperature fluctuations, from summer to autumn and winter, did induce spectral drift (Figure 4). Fortunately, this drift in the spectrum appears not to disrupt the signal intensity of individual energy peaks. Consequently, we have been able to correct for this drift by identifying characteristic energy peaks, including ^{40}K and low-energy backscattering. For this study we utilized software to automatically search for and define the characteristic energy peak of ^{40}K as a reference for energy peak drift correction. Following the subtraction of background interference from Compton photons and the removal of overlapping energy peaks using differential equations, we ultimately obtained a more precise estimate of nuclide activity concentration.

DOI: 10.29677/MR.202306_3(1).0002

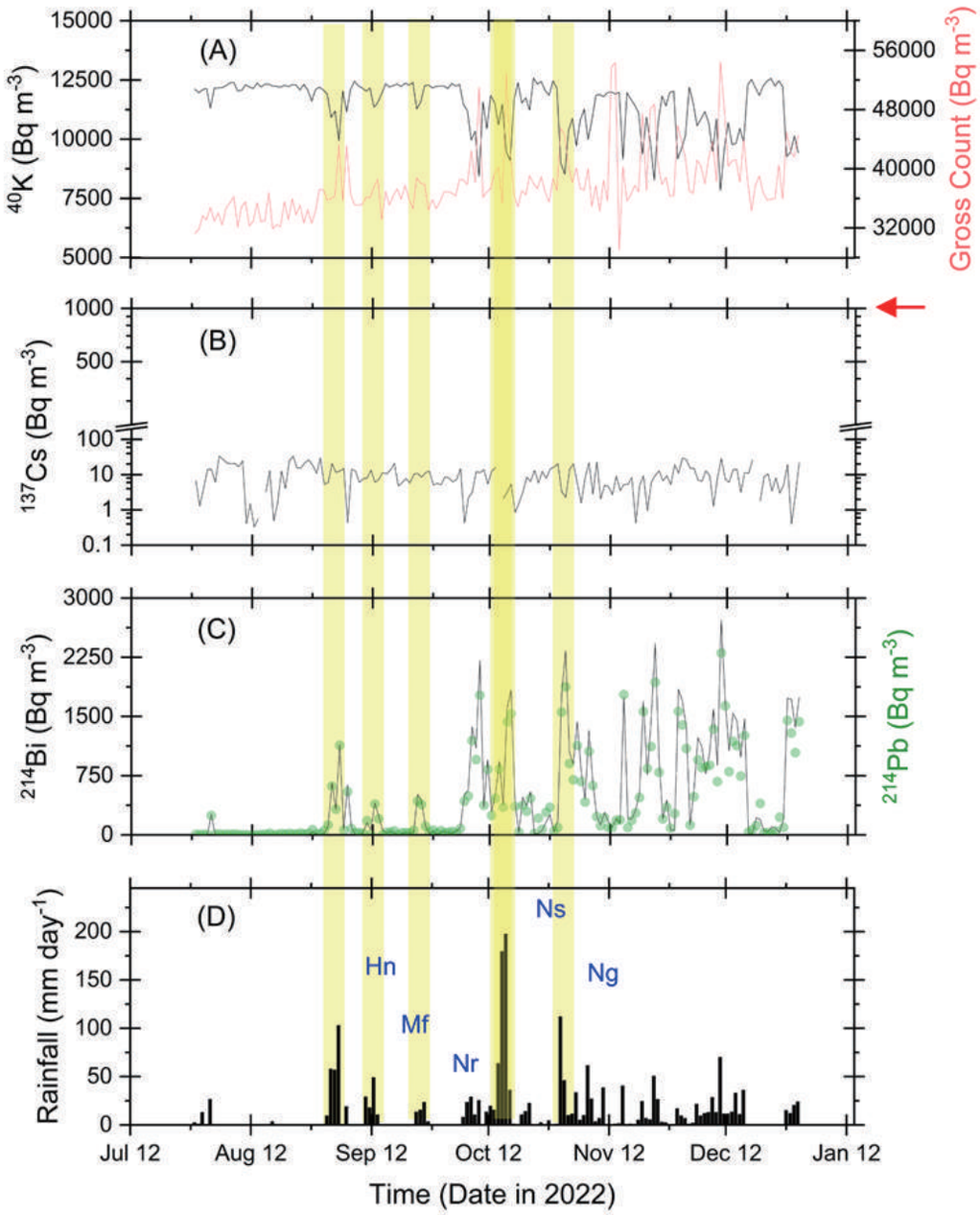

Figure 3. Temporal variations of (A) ^{40}K (in black) and gross count (in red), (B) ^{137}Cs, with an arrow indicating the WHO drinking water contamination standard for ^{137}Cs, (C) ^{214}Bi (black line) and ^{214}Pb (green dot), and (D) daily rainfall (data was obtained from the Dasi Fishing Harbor station operated by the Center Weather Administration, Taiwan); All data have been corrected for spectral interference and converted to activity concentration; Typhoons are highlighted with yellow backgrounds, including Hinnamnor (Hn), Mufa (Mf), Noru (Nr), Nesat (Ns), and Nalgae (Ng).

DOI: 10.29677/MR.202306_3(1).0002

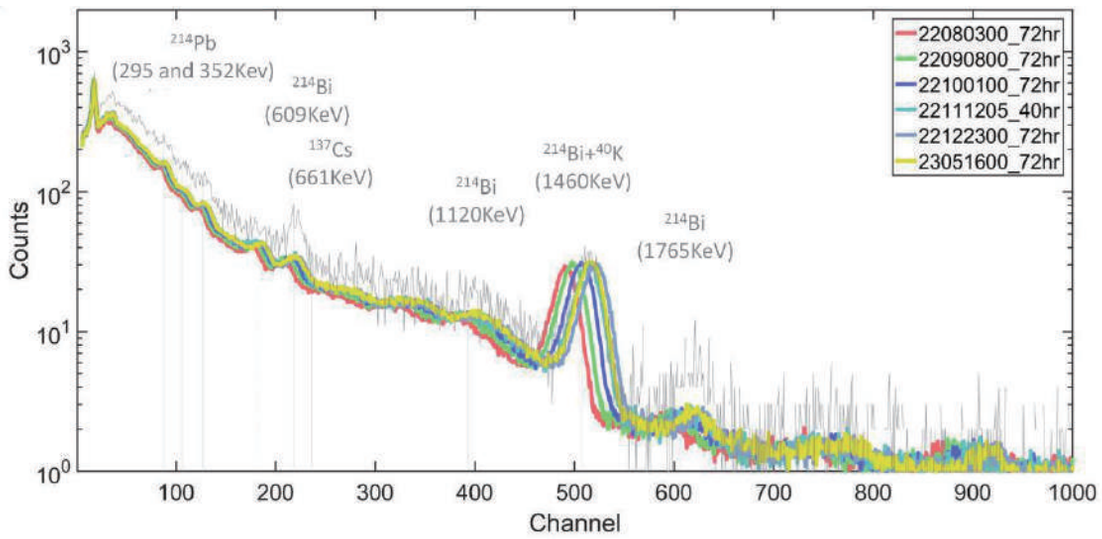

Figure 4. Spectral drift is observed across the 1,024 channels in the gamma spectrometer during the monitoring period from late July to the end of December in 2022; the grey curve represents a standard reference used to assess peak drift, encompassing both the Compton photon background and the marked characteristic peaks/nuclides.

Table 1. Monitoring data obtained from the gamma spectrometer and the temperature sensor equipped on the data buoy.

Time	Water Temperature	Gross Count	^{40}K	^{137}Cs	^{214}Bi	^{214}Pb	Accumulated Precipitation
	(°C)	Bq m^{-3}	Bq m^{-3}	Bq m^{-3}	Bq m^{-3}	Bq m^{-3}	mm
2022/7/29	28.933		12114	6.8	0	7	2.5
2022/7/30	29.029		11962	1.3	4	4	1.0
2022/7/31	29.121		12095	4.1	4	6	13
2022/8/1	29.004		12144	14	0	7	0.5
2022/8/2	28.696		11323	14	262	246	27
2022/8/3	28.863	33253	12149	6.1	1	7	0
2022/8/4	28.683	33168	12164	33	0	13	0
2022/8/5	28.813	32020	12178	27	0	2	0
2022/8/6	28.975	33497	12264	21	0	9	0
2022/8/7	28.767	33496	12378	21	0	4	0
2022/8/8	28.679	33383	12402	21	0	11	0
2022/8/9	28.775	33424	12042	17	0	5	0
2022/8/10	28.967	33502	12064	25	0	1	0
2022/8/11	28.417	33456	12301	0.4	4	0	0
2022/8/12	28.858	33539	12208	1.5	15	0	0

Marine Research of the National Academy of Marine Research
DOI: 10.29677/MR.202306_3(1).0002

Time	Water Temperature	Gross Count	^{40}K	^{137}Cs	^{214}Bi	^{214}Pb	Accumulated Precipitation
	(°C)	Bq m^{-3}	Bq m^{-3}	Bq m^{-3}	Bq m^{-3}	Bq m^{-3}	mm
2022/8/13	28.879	33676	12147	0.3	3	0	0
2022/8/14	28.871	33745	12367	0.6	8	0	0
2022/8/15	28.413	33775	12206	0	1	3	0
2022/8/16	28.271	32402	12326	3.3	4	7	0
2022/8/17	28.017	33957	12319	13	0	20	0
2022/8/18	27.604		12246	0.5	0	0	3.5
2022/8/19	28.288	32404	12228	1.6	11	5	0
2022/8/20	28.829	33786	12198	13	0	17	0
2022/8/21	29.546	33729	12275	4.1	7	9	0
2022/8/22	29.638	33860	12224	25	0	19	0
2022/8/23	29.363	33801	12298	34	0	11	0
2022/8/24	29.229	34016	12294	16	1	11	0
2022/8/25	29.113	34261	12076	16	1	23	0
2022/8/26	29.258	34231	12320	22	2	11	0
2022/8/27	29.208	34244	12072	26	2	20	0
2022/8/28	29.079	34397	11618	19	40	66	0
2022/8/29	29.046		12095	11	17	13	0.5
2022/8/30	29.308		12201	30	0	19	0.5
2022/8/31	28.683	34785	12079	5.3	19	55	0
2022/9/1	27.875		11909	6.0	111	125	9.5
2022/9/2	27.642		10924	21	656	617	58
2022/9/3	27.654		11186	12	321	325	57
2022/9/4	27.450		9955	13	1142	1135	103
2022/9/5	28.175	35349	12038	15	65	60	0
2022/9/6	28.067		11163	0.4	631	548	19
2022/9/7	27.800	35449	12111	15	96	80	0
2022/9/8	27.863	34672	12455	13	2	29	0
2022/9/9	28.025	34763	12252	6.0	0	31	0
2022/9/10	27.713	35011	12164	7.8	29	21	0
2022/9/11	27.492		12031	8.0	156	179	29
2022/9/12	26.971		12156	13	63	2	18
2022/9/13	26.492		11349	6.1	405	391	49

Marine Research of the National Academy of Marine Research
DOI: 10.29677/MR.202306_3(1).0002

Time	Water Temperature	Gross Count	^{40}K	^{137}Cs	^{214}Bi	^{214}Pb	Accumulated Precipitation
	(°C)	Bq m^{-3}	Bq m^{-3}	Bq m^{-3}	Bq m^{-3}	Bq m^{-3}	mm
2022/9/14	26.821		11550	7.3	239	204	11
2022/9/15	27.246	36209	11926	12	63	0	0
2022/9/16	27.092	35748	12342	11	24	33	0
2022/9/17	26.946	35822	12209	14	45	35	0
2022/9/18	27.333	36162	12273	21	23	51	0
2022/9/19	27.433	36229	12327	4.8	3	3	0
2022/9/20	26.942	35563	12222	5.9	17	28	0
2022/9/21	26.988	35685	12368	7.8	32	32	0
2022/9/22	27.229	35561	12284	5.8	23	23	0
2022/9/23	27.225	35510	12393	10	30	60	0
2022/9/24	26.883		11282	11	513	429	14
2022/9/25	26.688		11563	8.5	434	384	16
2022/9/26	27.338		12249	12	108	110	24
2022/9/27	27.425		12292	13	17	36	3.5
2022/9/28	26.913	35999	12166	5.1	46	62	0
2022/9/29	26.121	36142	12229	5.7	6	23	0
2022/9/30	26.004	36250	12247	5.2	37	54	0
2022/10/1	25.496	36175	12248	8.7	40	29	0
2022/10/2	25.625	35955	12140	8.1	26	35	0
2022/10/3	25.800	35737	12350	6.3	26	44	0
2022/10/4	25.875	35668	12243	7.3	44	23	0
2022/10/5	25.608		12320	14.9	96	82	0.5
2022/10/6	25.758		11464	0.4	507	426	8.0
2022/10/7	25.983		11209	2.2	564	493	24
2022/10/8	26.675		9964	3.1	1369	1194	29
2022/10/9	26.071		10341	12	1101	954	11
2022/10/10	25.383		8446	11	2206	1769	26
2022/10/11	24.833		11565	14	356	376	0.5
2022/10/12	24.779		10448	5.4	953	830	14
2022/10/13	24.338		11843	13	296	246	20
2022/10/14	24.017		11530	16	522	462	16
2022/10/15	23.500		10615	0.0	933	835	64

Marine Research of the National Academy of Marine Research
DOI: 10.29677/MR.202306_3(1).0002

Time	Water Temperature	Gross Count	^{40}K	^{137}Cs	^{214}Bi	^{214}Pb	Accumulated Precipitation
	(°C)	Bq m^{-3}	Bq m^{-3}	Bq m^{-3}	Bq m^{-3}	Bq m^{-3}	mm
2022/10/16	25.050		11471	2.1	379	351	180
2022/10/17	24.263		9461	3.2	1611	1431	198
2022/10/18	25.133		9108	5.4	1834	1536	36
2022/10/19	24.738		11684	0.9	416	359	1.0
2022/10/20	24.875	35260	12383	1.6	25	35	0
2022/10/21	25.233		11531	3.2	476	375	11
2022/10/22	24.729		11749	8.5	368	298	14
2022/10/23	22.921		11227	6.4	546	463	23
2022/10/24	22.850	35296	12580	13	14	20	0
2022/10/25	23.375	35367	12331	5.8	18	213	0
2022/10/26	23.471		12433	13	59	71	2.5
2022/10/27	23.596	36184	12038	7.9	164	287	0
2022/10/28	23.525		11860	15	257	349	4.5
2022/10/29	22.733	36083	12466	17	39	48	0
2022/10/30	22.854		12148	20	182	95	1.0
2022/10/31	23.629		8997	3.3	1785	1555	112
2022/11/1	24.688		8524	2.3	2332	1874	46
2022/11/2	24.146		10383	14	1049	903	10
2022/11/3	24.338		10870	21	900	698	12
2022/11/4	24.288		9727	5.7	1432	1133	34
2022/11/5	24.875		10808	1.6	822	675	5.0
2022/11/6	24.429		11268	8.4	453	416	10
2022/11/7	24.288		9996	22	1322	1058	62
2022/11/8	24.004		10798	2.8	676	623	27
2022/11/9	23.975		11856	23	238	232	3.5
2022/11/10	23.508		11888	2.1	128	117	7.0
2022/11/11	23.492		11797	5.0	284	219	39
2022/11/12	23.063	36849	11978	4.6	165	93	0
2022/11/13	23.900	37095	11988	2.7	101	93	0
2022/11/14	25.633		11917	9.1	205	184	1.0
2022/11/15	25.533		11984	3.6	149	189	1.5
2022/11/16	24.888		9153	5.3	1743	1777	41

Marine Research of the National Academy of Marine Research
DOI: 10.29677/MR.202306_3(1).0002

Time	Water Temperature	Gross Count	^{40}K	^{137}Cs	^{214}Bi	^{214}Pb	Accumulated Precipitation
	(°C)	Bq m^{-3}	Bq m^{-3}	Bq m^{-3}	Bq m^{-3}	Bq m^{-3}	mm
2022/11/17	24.833	37253	11961	5.3	208	93	0
2022/11/18	24.633		11682	8.3	201	184	1.0
2022/11/19	24.308	39244	11438	0.4	318	278	0
2022/11/20	23.713		11113	5.0	536	474	5.0
2022/11/21	23.983		9368	9.4	1694	1563	25
2022/11/22	23.838		10928	0.9	763	841	7.0
2022/11/23	22.654		9901	6.1	1467	1120	5.5
2022/11/24	22.642		8282	9.6	2425	1932	51
2022/11/25	23.054		10689	13.00	976	792	27
2022/11/26	22.621		11819	6.8	204	203	3.0
2022/11/27	22.504		11410	9.4	438	351	2.5
2022/11/28	23.025	37036	11976	5.3	61	87	0
2022/11/29	22.625	37151	12029	19	56	271	0
2022/11/30	21.333		9178	11	1845	1565	17
2022/12/1	21.258		9598	30	1697	1394	9.5
2022/12/2	21.233		10152	27	1365	1095	7.0
2022/12/3	21.238		12192	15	123	124	1.0
2022/12/4	21.242		11546	15	565	485	2.0
2022/12/5	21.063		10570	7.1	1232	953	22
2022/12/6	21.538		10848	6.5	1117	851	9.5
2022/12/7	22.188		11164	13	778	866	12
2022/12/8	22.471		10686	9.5	1040	884	13
2022/12/9	22.017		9486	1.3	1592	1342	29
2022/12/10	22.879		10851	8.4	883	675	13
2022/12/11	22.338		7842	28	2724	2304	70
2022/12/12	22.104		9606	7.5	1691	1634	12
2022/12/13	22.708		10691	6.1	1067	800	12
2022/12/14	22.808		9780	14	1541	1185	14
2022/12/15	23.442		9829	14	1446	1130	33
2022/12/16	22.983		10453	3.2	984	745	11
2022/12/17	21.029		9876	12	1468	1259	36
2022/12/18	21.858	35992	12299	11	19	35	0

Marine Research of the National Academy of Marine Research
DOI: 10.29677/MR.202306_3(1).0002

Time	Water Temperature	Gross Count	^{40}K	^{137}Cs	^{214}Bi	^{214}Pb	Accumulated Precipitation
	(°C)	Bq m^{-3}	Bq m^{-3}	Bq m^{-3}	Bq m^{-3}	Bq m^{-3}	mm
2022/12/19	22.558	36000	12524	26	20	66	0
2022/12/20	22.283	37165	12165	0.0	218	120	0
2022/12/21	20.525	38058	11858	1.8	195	398	0
2022/12/22	19.713	36794	12246	8.8	50	29	0
2022/12/23	19.813	36551	12455	11	41	32	0
2022/12/24	20.350	36497	12566	3.5	104	17	0
2022/12/25	21.321	36541	12247	8.1	84	50	0
2022/12/26	21.008	36594	12472	3.0	29	224	0
2022/12/27	21.017	37108	12228	5.2	196	95	0
2022/12/28	21.213		9269	20	1732	1450	15
2022/12/29	20.529		9453	0.4	1719	1291	12
2022/12/30	20.746		10135	2.7	1364	1042	21
2022/12/31	21.309		9422	22	1743	1434	24
Average	25.291		11451	10.1	481	417	13
±SD	2.739		1079	7.7	639	532	27
Average (no rain)	26.264	33608	12212	11	43	54	
±SD	2.919	620	195	8	64	78	

3.1 Time-series variation of ^{137}Cs

We performed the integration of gamma spectra from the northeastern coast of Yilan at the buoy monitoring station. However, the characteristic energy peak at 661 keV did not reveal a clear ^{137}Cs peak, regardless of whether we integrated the data over 12 hours, 24 hours, 36 hours, or 48 hours. This suggests that the ^{137}Cs activity concentration in the seawater of this region falls below the lower detection limit of the instrument, which is 30 Bq m^{-3}. This level of the detection limit is attributed to the tailing background signal at the Compton edge and the insufficient detection resolution of the crystal. Consequently, we opted to analyze the data by converting the 24-hour integration data into hourly activity concentrations, reducing counting errors per hour and enhancing statistical significance. The average ^{137}Cs value from July 29 to December 30 was 10.1±7.7 Bq m^{-3} (mean±SD, n=156) (Figure 3B). Notably, this result exceeds the actual ^{137}Cs level in the study area (Huang et al., 2021), indicating that the NaI(Tl) detector is inadequate for accurately quantifying low-concentration ^{137}Cs in the environment during periods without marine radiation pollution events. While we have corrected the ^{137}Cs data for spectral interference from Compton photons and ^{214}Bi tailing, some noise induced by rainfall remains unavoidable, particularly during non-typhoon rainfall periods. The inaccurate measurement of ^{137}Cs is primarily attributed to the high lower detection limit (LOD) of the instrument and consequently, a high limit of quantification (LOQ). We anticipate that the quantitative results will become more accurate once the radioactivity levels exceed 90 Bq m^{-3} or even 150 Bq m^{-3} (3 to 5 times of the LOD).

Marine Research of the National Academy of Marine Research
DOI: 10.29677/MR.202306_3(1).0002

The main reason for our inability to measure ^{137}Cs activity concentration in seawater is the normal value of ^{137}Cs in the surface seawater off the coast of Yilan or the Kuroshio Current extending to the eastern coast of Taiwan, which is approximately 1.0±0.3 Bq m^{-3} (Huang et al., 2021; Wu et al., 2020). This concentration level significantly falls below the lower detection limit of the instrument. Nevertheless, the primary objective of establishing the in situ automated gamma radioactivity monitoring buoy station is to furnish early warnings for abnormal gamma radiation in the marine environment. The absence of ^{137}Cs signals under normal conditions signifies the absence of concerns regarding gamma radiation contamination in the surface seawater off the coast of Yilan or the Kuroshio surface water.

The gamma radioactivity spectrometer employed in this study is of the standard type (non-high sensitivity). Although its detection limit does not meet the background survey requirements for ^{137}Cs activity concentration in the territorial waters off Taiwan, it still possesses substantial capabilities for early warning of radiation anomalies. These anomalies could include nuclear power plant accidents, marine leakage, nuclear waste disposal, and offshore nuclear tests. In the future, if the need for the detection of low activity concentrations arises, the instrument can be replaced with a high-sensitivity model (featuring a larger crystal) to potentially reduce the detection limit to 5 Bq m^{-3} or lower.

3.3 Feasibility of estimating rainfall with ^{214}Pb and ^{214}Bi

Previous research has consistently documented that rainfall precipitation can result in an elevation of the gross gamma count in seawater, primarily attributable to increased levels of natural radioisotopes ^{214}Pb and ^{214}Bi. This phenomenon stems from the introduction of radon gas from the atmosphere to the sea surface during rainfall, which, through the decay of its daughter isotopes ^{214}Pb and ^{214}Bi, subsequently augments the gross gamma count in seawater (Patiris et al., 2021; Tsabaris et al., 2021). The decay sequence initiates with radon-222 (^{222}Rn, with a half-life of 3.8 days), progressing to polonium-218 (^{218}Po, with a half-life of 3.1 minutes). This process further involves decay to ^{214}Pb (with a half-life of 26.8 minutes), subsequent decay to ^{214}Bi (with a half-life of approximately 19.9 minutes), and ultimately concluding with the decay to stable lead-206 (^{206}Pb). Importantly, throughout this decay sequence, the decay of ^{214}Pb and ^{214}Bi is accompanied by gamma radiation, with ^{214}Pb exhibiting major gamma energy peaks at 295 and 352 keV, and ^{214}Bi displaying major gamma energy peaks at 609 and 1,764 keV.

Our data confirm a clear relationship between ^{214}Pb, ^{214}Bi, and the gross gamma count with rainfall events (Figure 3C and 3D). The data reveals a highly positive correlation between the daily cumulative counts of ^{214}Bi and ^{214}Pb during the monitoring period (r=0.996, n=156). Additionally, daily cumulative rainfall accurately mirrors the daily average rainfall (r=1.000, n=94). Considering that ^{214}Pb is susceptible to significant interference from signals resulting from low-energy backscattering, we have opted to discuss the correlation using the daily cumulative count of ^{214}Bi and the daily cumulative rainfall. The observed fluctuations in ^{214}Bi during rainfall events, alongside the moderate correlation between ^{214}Bi and rainfall (r=0.448, n=94), serve as confirmation of the relationship between ^{214}Pb, ^{214}Bi, and rainfall in the surface seawater of the study area.

We have conducted a comparative analysis of the relationship between ^{214}Bi and both general rainfall and typhoon-induced rainfall using the same set of monitoring data (Figure 5). Our analysis assumes that ^{222}Rn levels in the atmosphere remain relatively constant within the same season (Moriizumi et al., 2008). During non-typhoon periods, ^{214}Bi exhibits a strong positive correlation with rainfall (r=0.704, n=79), primarily reflecting rainfall events associated with the prevailing East Asian winter monsoon, which occur from late autumn to winter. These rainfall events are characterized by extended durations (spanning several consecutive days) but low rainfall intensity, averaging 13.0±14.5 mm (mean±1SD). In contrast, during typhoon periods, such as Typhoon Hinnamnor and Typhoon Mufa, which followed a trajectory along the eastern Kuroshio Current and brushed past the Yilan oceanic region, a high correlation with accumulated rainfall is evident, with correlation coefficients of r=0.980 (n=3) and 0.641 (n=3), respectively. Notably, the other three typhoons,

DOI: 10.29677/MR.202306_3(1).0002

including Typhoon Noru, Typhoon Nesat, and Typhoon Nalgae, which traversed the eastern side of Luzon (off Southern Taiwan) from the Western Pacific Ocean before entering the South China Sea, exhibited no significant relationship between surface seawater ^{214}Bi activity concentration and rainfall during their respective periods. However, it is important to highlight that Typhoons Nesat and Nalgae resulted in substantial rainfall in the Yilan region, with the daily cumulative ^{214}Bi activity concentrations surpassing those observed during Typhoon Hinnamnor when it approached Taiwan. Although we currently lack a definitive explanation for this 'excess ^{214}Bi,' it can be inferred from the typhoon paths that this excess may be associated with moisture carried by the outer circulation of the typhoons. This moisture potentially contains additional ^{214}Bi. Furthermore, our observations reveal that, during various rainfall events, the highest activity concentrations of ^{214}Bi do not necessarily coincide with the peak of rainfall; at times, there is a delay, and the levels rapidly return to background levels after rainfall cessation. This delayed phenomenon may be indicative of contributions from land-based surface runoff or the transport of ^{214}Bi by surface currents from adjacent regions due to the extensive coverage of rainfall or distinct rain cells within the same event. These hypotheses warrant further validation in future studies. Similar delayed occurrences of ^{214}Bi during rainfall have been observed elsewhere (Bottardi et al., 2020; Patiris et al., 2021). However, our observations do not support the notion that ^{222}Rn needs time for decay to produce this delay (Patiris et al., 2021). Instead, our data suggest that a substantial amount of ^{214}Bi and ^{214}Pb may already exist in atmospheric aerosol particles before the onset of rainfall.

Prior research has directly utilized ^{214}Bi and ^{214}Pb to estimate the increase in gamma dose rates resulting from natural gamma radiation due to rainfall or to estimate atmospheric ^{222}Rn (Ambrosino et al., 2020; Bottardi et al., 2020). Based on our initial observations, future investigations may contemplate additional factors, such as rainfall intensity, surface runoff into the ocean, and the concentration of fine atmospheric aerosol particles (e.g., $PM_{2.5}$) during individual rainfall events, to accurately estimate the natural gamma dose rate. This endeavor can build upon the existing framework established by previous studies.

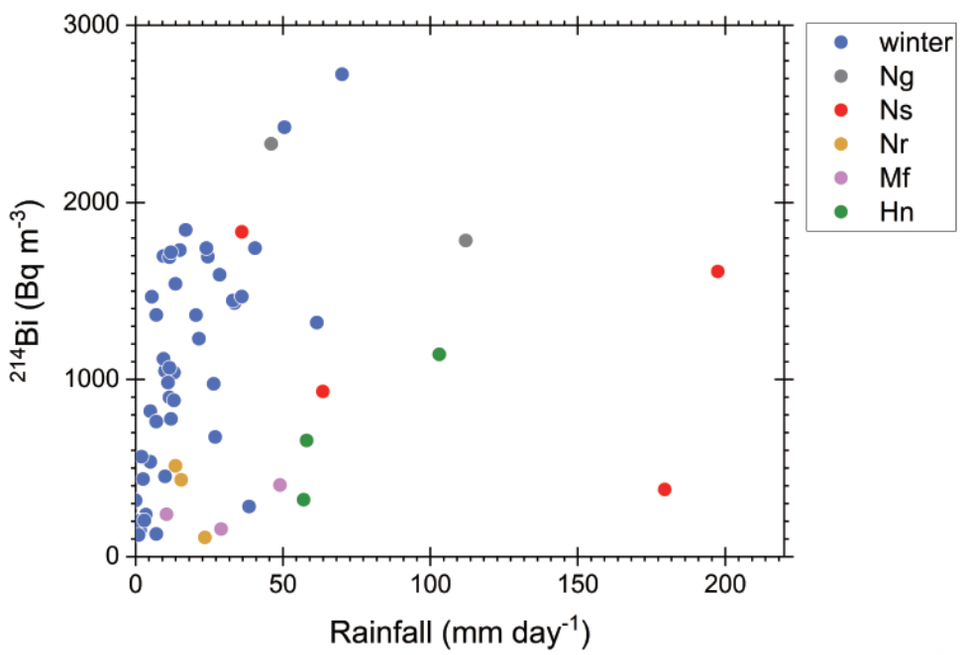

Figure 5. Radon progeny ^{214}Bi activity concentration over daily accumulated rainfall; Symbols represent typhoons Hinnamnor (Hn), Mufa (Mf), Noru (Nr), Nesat (Ns), and Nalgae (Ng), as well as the rainfall occurring during the prevailing East Asian winter monsoon.

Marine Research of the National Academy of Marine Research
DOI: 10.29677/MR.202306_3(1).0002

3.4 Public information display platform and future planning

The primary objective behind establishing the sea-based, in situ automated gamma radioactivity monitoring buoy station in this study is to address public concerns in Taiwan arising from the potential release of tritium-containing water from the Fukushima Daiichi Nuclear Power Plant. By providing scientific monitoring results, this initiative aims to mitigate apprehensions related to the presence of residual radioactive substances beyond tritium in the released water. Furthermore, the introduction of advanced monitoring instruments and technologies enhances Taiwan's capacity for radiation monitoring in the marine environment. Currently, the operation of the in situ automated gamma radioactivity monitoring buoy station proceeds smoothly, with all monitoring data transmitted via 4G to the database of the National Academy of Marine Research. The time-series variations of ^{137}Cs monitoring values in the waters off the northeastern coast of Yilan are accessible through the National Ocean Database and Sharing System (NODASS) platform (https://nodass.namr.gov.tw/) (Figure 1D). Additionally, the relevant data may be accessible on the GoOcean platform (https://goocean.namr.gov.tw/), which offers marine recreation risk information to the public.

In the future, our plan is to expand the monitored oceanic areas and proactively prepare for potential risks associated with nuclear power plants in neighboring countries. This will enable us to utilize the monitoring system as needed and overcome the limitations of the current traditional approach, which involves collecting seawater samples every three months. The traditional method primarily serves as a 'historical record' for assessing background radiation in the marine environment at three-month intervals, lacking the capability to detect marine radiation pollution in real time. Moreover, the process of collecting seawater samples necessitates their transportation back to the laboratory, consuming both time and human resources for subsequent processing and analysis. Additionally, personnel involved in sample collection are exposed to potential radiation contamination risks in the field, which may remain unknown at the time of sampling. In comparison to the seasonal marine radioactivity surveys currently conducted by the Atomic Energy Council and its affiliated institutions of Taiwan, the establishment of our in situ automated gamma radioactivity mooring buoy station is a noteworthy achievement. It showcases Taiwan's ability to engage in in situ, near-continuous monitoring and near-real-time remote transmission of ^{137}Cs gamma radiation data in marine areas.

4 CONCLUSIONS

We have successfully deployed a marine, in-situ automated gamma radioactivity monitoring buoy station off the northeastern coast of Yilan, Taiwan, since the end of July 2022. It has operated smoothly for the past five months, concluding at the end of December 2022. The continuous automatic gamma spectrum data have been successfully transmitted to the onshore data receiving station via 4G, and the gamma energy peaks have been automatically converted into activity concentrations. The data are archived in the NODASS, and the ^{137}Cs data is also publicly available through the NODASS website platform. It is important to reiterate that the purpose of establishing the in situ seawater radioactivity monitoring system is to facilitate the prompt response to unidentified nuclear accidents through the monitoring system's alarm system, rather than replacing traditional laboratory testing.

The in situ automatic monitoring of gamma radiation data in this study's area revealed the following:

1. The total counts and ^{40}K reflect good instrument stability, as well as high accuracy and precision of measurements.

2. The anthropogenic radionuclide ^{137}Cs in the surface seawater off the coast of Yilan is below the instrumental detection limit of 30 Bq m^{-3} (past monitoring data by water sampling indicates local seawater is around 1.0 Bq m^{-3}), which is much lower than the WHO drinking water standard of 10,000

Marine Research of the National Academy of Marine Research
DOI: 10.29677/MR.202306_3(1).0002

Bq m^{-3}. This instrument is suitable for detecting nuclear pollution in seawater and is not intended for measuring low-concentration seawater radiation background values.

3. The activity concentrations of the natural radionuclides ^{214}Pb and ^{214}Bi demonstrated an elevation during rainfall events and remained thereafter, leading to an increase in the total gamma radiation counts. Based on existing evidence, we speculate that the relationship between rainfall and ^{214}Bi or ^{214}Pb radiation doses is not solely determined by rainfall volume, but also influenced by factors such as nearby surface runoff, different rainfall cells, surface ocean currents, and atmospheric aerosol concentration.

The establishment of the automated gamma radioactivity monitoring buoy station in this sea area has achieved automatic and near-continuous monitoring of marine gamma radioactivity in near real time. This lays the foundation for the development of a diversified underwater Internet of Things and provides enhanced security for maritime users. This study has successfully established Taiwan's first maritime gamma radiation monitoring station, demonstrating the technical capability of Taiwan for long-term, near-real-time automatic monitoring of marine gamma radioactivity. In the next phase, we will attempt to improve buoy power to enable the observation of other marine environmental parameters and develop in situ detection techniques for beta (β) radiation. We also hope that with this successful example, we can expand monitoring stations in various critical sea areas in the future to serve as a mechanical sentinel for monitoring potential marine radiation pollution. In combination with nowcast and forecast numerical models for the marine transport of radioactive substances, we aim to further enhance Taiwan's warning capabilities for offshore marine radiation and ensure public health and safety.

ACKNOWLEDGEMENTS

We would like to express our gratitude to the COMC team for their assistance in the installation and deployment of the buoy system, as well as their support in data quality control. We thank Nijin Environmental Technology Co., Ltd., for providing maintenance for the gamma spectrometers and related technical services free of charge. We are grateful to the NODASS team of the NAMR in collaboration with GeoNet Co., Ltd., for their assistance in data archiving and website display. We extend special thanks to former NAMR President Yung-Fang Chiu for his strong support of this project, as well as to the INER, AEC for their technical guidance and suggestions on gamma spectrometry. This project was funded by the National Development Fund, Executive Yuan, and the NAMR's annual budget.

DOI: 10.29677/MR.202306_3(1).0002

REFERENCES

Ambrosino, F., Thinová, L., Hýža, M., & Sabbarese, C. (2020). ^{214}Bi/^{214}Pb radioactivity ratio three-year monitoring in rainwater in Prague. *Nukleonika, 65*(2), 115-119. https://doi.org/10.2478/nuka-2020-0018

Aoyama, M., Hirose, K., Nemoto, K., Takatsuki, Y., & Tsumune, D. (2008). Water masses labeled with global fallout ^{137}Cs formed by subduction in the North Pacific. *Geophysical Research Letters, 35*(1). https://doi.org/10.1029/2007gl031964

Behrens, E., Schwarzkopf, F. U., Lübbecke, J. F., & Böning, C. W. (2012). Model simulations on the long-term dispersal of ^{137}Cs released into the Pacific Ocean off Fukushima. *Environmental Research Letters, 7*(3), 034004. http://dx.doi.org/10.1088/1748-9326/7/3/034004

Bailly du Bois, P., Dumas, F., Voiseux, C., Morillon, M., Oms, P. E., & Solier, L. (2020). Dissolved radiotracers and numerical modeling in north European continental shelf dispersion studies (1982–2016): Databases, methods and applications. *Water, 12*(6), 1667. https://doi.org/10.3390/w12061667

Bottardi, C., Albéri, M., Baldoncini, M., Chiarelli, E., Montuschi, M., Raptis, K. G. C., Serafini, A., Strati, V., & Mantovani, F. (2020). Rain rate and radon daughters' activity. *Atmospheric Environment, 238,* 117728. https://doi.org/10.1016/j.atmosenv.2020.117728

Buesseler, K. O. (2014). Fukushima and ocean radioactivity. O*ceanography, 27*(1), 92-105. https://doi.org/10.5670/oceanog.2014.02

Buesseler, K., Dai, M., Aoyama, M., Benitez-Nelson, C., Charmasson, S., Higley, K., Maderich, V., Masqué, P., Morris, P. J., Oughton, D., & Smith, J. N. (2016). Fukushima Daiichi–derived radionuclides in the ocean: Transport, fate, and impacts. *Annual Review of Marine Science, 9*(1), 173-203. https://doi.org/10.1146/annurev-marine-010816-060733

Burr, G. S., Matsuzaki, H., Wang, B. S., Kusuno, H., Tokuyama, H., Yamagata, T., Yu, T. L., Wang, S. L., Chang, C. C., Jull, A. J. T., & Lo, C. H. (2020). Anthropogenic ^{129}I in the South China Sea and coastal waters around Taiwan. *Elementa: Science of the Anthropocene, 8*(1). https://doi.org/10.1525/elementa.2020.064

Choi, Y., Ji, Y. Y., & Joung, S. (2023). Experimental counting efficiency calibration of In Situ marine radioactivity monitoring systems in Busan (Korea) based on seawater salinity. *Journal of Coastal Research, 39*(2), 377-383. https://doi.org/10.2112/jcoastres-d-22tm-00013.1

Doong, D. J., Chen, S. H., Kao, C. C., Lee, B. C., & Yeh, S. P. (2007). Data quality check procedures of an operational coastal ocean monitoring network. *Ocean Engineering, 34*(2), 234-246. https://doi.org/10.1016/j.oceaneng.2006.01.011

Dou, D., Zeng, Z., Yu, W., Zeng, M., Men, W., Lin, F., Ma, H., Cheng, J., & Li, J. (2021). In-situ seawater gamma spectrometry with $LaBr_3$ detector at a nuclear power plant outlet. *Journal of Marine Science and Engineering, 9*(7), 721. https://doi.org/10.3390/jmse9070721

Huang, W. J., Lee, M. T., Huang, K. C., Kao, K. J., Lee, M. A., Yang, Y. J., Jan, S., & Chen, C. T. A. (2021). Radiocesium in the Taiwan Strait and the Kuroshio east of Taiwan from 2018 to 2019. *Scientific Reports, 11*(1), 22467. https://doi.org/10.1038/s41598-021-01895-y

Inomata, Y., Aoyama, M., & Hirose, K. (2008). Analysis of 50-y record of surface ^{137}Cs concentrations in the global ocean using the HAM-global database. *Journal of Environmental Monitoring, 11*(1), 116-125. https://doi.org/10.1039/b811421h

Kalfas, C. A., Axiotis, M., & Tsabaris, C. (2016). SPECTRW: A software package for nuclear and atomic spectroscopy. Nuclear Instruments and Methods in Physics Research Section A: Accelerators, Spectrometers, Detectors and Associated Equipment, 830, 265-274. https://doi.org/10.1016/j.nima.2016.05.098

Kao, C. C., Doong, D. J., Hsin Chuang, L. Z., & Lee, B. C. (2003, May 25-30). Automatic quality check method on in-situ data from the coastal ocean monitoring net around Taiwan [Conference presentation: ISOPE-I-03-228]. The Thirteenth International Offshore and Polar Engineering Conference, Honolulu, Hawaii, USA.

Kumagai, H., Iwase, R., Kinoshita, M., Machiyama, H., Hattori, M., & Okano, M. (2012). Environmental gamma-ray observation in deep sea. In F. Adrovic (Ed.), *Gamma radiation*. InTech. https://doi.org/10.5772/36392

Kumamoto, Y., Aoyama, M., Hamajima, Y., Nagai, H., Yamagata, T., Kawai, Y., Oka, E., Yamaguchi, A., Imai, K., & Murata, A. (2017). Fukushima-derived radiocesium in the western North Pacific in 2014. *Journal of Radioanalytical and Nuclear Chemistry, 311*(2), 1209-1217. https://doi.org/10.1007/s10967-016-5055-3

Kwak, S. W., Choi, J., Park, S. S., Ahn, S. H., Park, J. S., & Chung, H. (2017). Comparison of experimental results of a Quad-CZT array detector, a NaI(Tl), a $LaBr_3$(Ce), and a HPGe for safeguards applications. *Journal of Instrumentation, 12*(11), C11011. https://doi.org/10.1088/1748-0221/12/11/C11011

Men, W., He, J., Wang, F., Wen, Y., Li, Y., Huang, J., & Yu, X. (2015). Radioactive status of seawater in the northwest Pacific more than one year after the Fukushima nuclear accident. *Scientific Reports, 5,* 7757. https://doi.org/10.1038/srep07757

Moriizumi, J., Ohkura, T., Hirao, S., Nono, Y., Yamazawa, H., Kim, Y. S., Guo, Q., Mukai, H., Tohjima, Y., & Iida, T. (2008). Continuous observation of atmospheric ^{222}Rn concentrations for analytic basis of atmospheric transport in East Asia. *Journal of Nuclear Science and Technology, 45*(sup6), 173-179. https://doi.org/10.1080/00223131.2008.10876002

Patiris, D. L., Pensieri, S., Tsabaris, C., Bozzano, R., Androulakaki, E. G., Anagnostou, M. N., & Alexakis, S. (2021). Rainfall investigation by means of marine in situ gamma-ray spectrometry in Ligurian Sea, Mediterranean Sea, Italy. *Journal of Marine Science and Engineering, 9*(8), 903. https://doi.org/10.3390/jmse9080903

Pensieri, S., Patiris, D., Alexakis, S., Anagnostou, M. N., Prospathopoulos, A., Tsabaris, C., & Bozzano, R. (2018). Integration of underwater radioactivity and acoustic sensors into an open sea near real-time multi-parametric observation system. *Sensors, 18*(8), 2737. https://doi.org/10.3390/s18082737

Povinec, P. P., & Hirose, K. (2012). Radionuclides as Tracers of Ocean Currents. In Meyers, R.A. (Eds), *Encyclopedia of Sustainability Science and Technology.* Springer, New York. https://doi.org/10.1007/978-1-4419-0851-3_289

Ren, G. X., Wei, Z. Q., Liu, D. Y., & Zhang, Y. Y. (2017). Marine radioactive field monitoring sensor based on NaI (Tl). *IOP Conference Series: Earth and Environmental Science, 82*(1), 012088. https://doi.org/10.1088/1755-1315/82/1/012088

Santschi, P. H. (2018). Marine colloids, agents of the self-cleansing capacity of aquatic systems: Historical perspective and new discoveries. *Marine Chemistry, 207*, 124-135. https://doi.org/10.1016/j.marchem.2018.11.003

Topcuoğlu, S. (2001). Bioaccumulation of cesium-137 by biota in different aquatic environments. *Chemosphere, 44*(4), 691-695. https://doi.org/10.1016/s0045-6535(00)00290-3

Tracy, B. L., Carini, F., Barabash, S., Berkovskyy, V., Brittain, J. E., Chouhan, S., Eleftheriou, G., Iosjpe, M., Monte, L., Psaltaki, M., Shen, J., Tschiersch, J., & Turcanu, C. (2013). The sensitivity of different environments to radioactive contamination. *Journal of Environmental Radioactivity, 122,* 1-8. https://doi.org/10.1016/j.jenvrad.2013.02.015

Tsabaris, C., Androulakaki, E. G., Ballas, D., Alexakis, S., Perivoliotis, L., & Iona, A. (2021). Radioactivity monitoring at North Aegean Sea integrating in-situ sensor in an ocean observing platform. *Journal of Marine Science and Engineering, 9*(1), 77. https://doi.org/10.3390/jmse9010077

Wu, J. (2018). Impacts of Fukushima Daiichi Nuclear Power Plant accident on the Western North Pacific and the China Seas: Evaluation based on field observation of ^{137}Cs. *Marine Pollution Bulletin, 127,* 45-53. https://doi.org/10.1016/j.marpolbul.2017.11.056

Wu, J., Xiao, X., & Sun, J. (2020). Distribution and budget of ^{137}Cs in the China Seas. *Scientific Reports, 10*(1), 8795. https://doi.org/10.1038/s41598-020-65280-x

Yu, S., Yarlagadda, B., Siegel, J. E., Zhou, S., & Kim, S. (2020). The role of nuclear in China's energy future: Insights from integrated assessment. *Energy Policy, 139,* 111344. https://doi.org/10.1016/j.enpol.2020.111344